Measurements and model comparisons suggest that HONO may not be an important source of OH radicals below a rural forest canopy

Bode Hoover,[a] Emily Reidy,[b] Ian Spink,[a] Amanda Hamachek,[b] Brandon Bottorff,[b] Philip S. Stevens,[ab*]

[a]O'Neill School of Public and Environmental Affairs, Indiana University, Bloomington, IN, U.S.A.

[b]Department of Chemistry, Indiana University, Bloomington, IN, U.S.A.

Supplemental Material

Text S1-S2

Tables S1-S5

Figures S1-S10

Text S1: Calculations of HONO sources

For the homogeneous reaction between OH and NO (P_{OH+NO}), the high and low pressure limit JPL rate constants (cm^3 $molecules^{-1}$ s^{-1})[1] are used along with measured OH (molecules cm^{-3}) and the estimated NO obtained by scaling the measured NO_2 (ppb) by the measured NO/NO_2 ratio from 2016.[2]

$$P_{OH+NO} = k_{OH+NO}[OH][NO] \quad \text{(ES1)}$$

Direct vehicle emissions and soil emissions were not included in the model. The rural forest location (Fig. S1) was at least 5.5 km from the nearest town of Pellston, MI which has a small population. The photolysis of adsorbed particulate nitrate ($P_{HNO_3+\,hv}$) was modeled by

$$P_{HNO_3+\,hv} = J_{HNO_3}[HNO_3]EF \quad \text{(ES2)}$$

where $[HNO_3]$ is the F0AM modeled concentration of nitric acid, J_{HNO_3} is the photolysis frequency of atmospheric HNO_3 calculated by the NCAR TUV model and scaled by J_{corr}, and EF is the enhancement factor for the photolysis frequency which was set to 30 due to the faster photolysis rate of particle phase HNO_3 than gas phase.[3,4]

Production of HONO from the heterogeneous conversion of NO_2 on surfaces was divided into ground and aerosol surfaces along with photoenhanced versions of each. The production on ground surfaces (P_{ground}) and its photoenhanced reaction ($P_{ground+hv}$) are modeled by

$$P_{ground} = \frac{\gamma_{NO_2}\nu_{NO_2}}{8}\frac{S_{ground}}{V}\frac{RH}{50}[NO_2] \quad \text{(ES3)}$$

$$P_{ground+hv} = P_{ground}\frac{\gamma_{NO_2,hv}}{\gamma_{NO_2}}\left(\frac{J_{NO_2}}{\beta}\right)^3 \quad \text{(ES4)}$$

where $[NO_2]$ is the measured NO_2 concentration (ppb), γ_{NO_2} is the uptake coefficient of NO_2 on the ground surface (dimensionless), $\gamma_{NO_2,h\nu}$ is the photoenhanced uptake coefficient (dimensionless), J_{NO_2} is the measured photolysis frequency of NO_2, β is the photohenhancement factor (dimensionless), RH is the measured relative humidity (%), and $\frac{S_{ground}}{V}$, is the calculated surface area to volume ratio for ground surfaces (m^{-1}) based on an estimated boundary layer height (m).[5–7] The average pH at this site (5.98) indicated there would be minimal conversion of nitrite to HONO according to Henry's Law.

Production on aerosol surfaces ($P_{aerosol}$) and its photoenhanced reaction ($P_{aerosol+h\nu}$) are modeled by

$$P_{aerosol} = \frac{\gamma_{NO_2} v_{NO_2}}{4} \frac{S_{aerosol}}{V} [NO_2] \quad \text{(ES5)}$$

$$P_{aerosol+h\nu} = P_{aerosol} \frac{\gamma_{NO_2,h\nu}}{\gamma_{NO_2}} \frac{J_{NO_2}}{\beta} \quad \text{(ES6)}$$

where $[NO_2]$ is the measured NO_2 concentration (ppb), γ_{NO_2} is the uptake coefficient of NO_2 on the ground surface (dimensionless), v_{NO_2} is the molecular speed of NO_2 (m s^{-1}), $\gamma_{NO_2,h\nu}$ is the photoenhanced uptake coefficient (dimensionless), J_{NO_2} is the measured photolysis frequency of NO_2 (s^{-1}), RH is the measured relative humidity (%), and $\frac{S_{aerosol}}{V}$ is the estimated constant surface area to volume ratio for aerosol surfaces (m^{-1}). The dimensionless photoenhancement factor (β) is calculated by

$$\beta = \frac{J_{NO_2\,max}}{J_{NO_2\,min}} \quad \text{(ES7)}$$

Other minor production mechanisms including the hydroperoxyl-water complex ($P_{HO_2 \cdot H_2O+NO_2}$), HO_2NO_2 decomposition ($P_{HO_2NO_2}$), the photolysis of orthonitrophenols ($P_{C_6H_5NO_3+hv}$), and the hydrolysis of NO_x on surfaces (P_{NOx}) were modeled by

$$P_{HO_2 \cdot H_2O+NO_2} = k_{HO_2 \cdot H_2O+NO_2}[HO_2 \cdot H_2O][NO_2] \quad \text{(ES8)}$$

$$P_{HO_2NO_2} = k_{HO_2NO_2}[HO_2NO_2] \quad \text{(ES9)}$$

$$P_{C_6H_5NO_3+hv} = J_{C_6H_5NO_3}[C_6H_5NO_3] \quad \text{(ES10)}$$

$$P_{NO_x} = k_{NO+NO_2+H_2O}[NO][NO_2][H_2O] \quad \text{(ES11)}$$

where $[NO_2]$ is the measured NO_2 concentration (ppb), $[HO_2 \cdot H_2O]$ is the F0AM modeled $HO_2 \cdot H_2O$ concentration (molecules cm^{-3}), $k_{HO_2 \cdot H_2O+NO_2}$ is the rate constant for the reaction (2.1×10^{-25}),[8,9] $[HO_2NO_2]$ is the modeled HO_2NO_2 concentration, $k_{HO_2NO_2}$ is the upper limit rate constant for the decomposition of HO_2NO_2 (5×10^{-16}),[1] $[C_6H_5NO_3]$ is the constant 1 ppb concentration of the class of orthonitrophenols,[10] $J_{C_6H_5NO_3}$ is the calculated photolysis frequency of orthonitrophenols scaled by J_{corr} (s^{-1}), $k_{NO+NO_2+H_2O}$ is the rate constant for the reaction between NO, NO_2 and H_2O to form HONO (6.06×10^{-38}).[11] These minor production pathways were combined in the main paper as P_{other} (ES12).

$$P_{other} = P_{HO_2 \cdot H_2O+NO_2} + P_{HO_2NO_2} + P_{C_6H_5NO_3+hv} + P_{NO_x} + P_{aerosol} + P_{aerosol+hv} + P_{ground+hv} + P_{ground+hv} + P_{HNO_3+hv} \quad \text{(ES12)}$$

Text S2: Calculations of HONO sinks

The major HONO sinks are described in detail in the main text. Here, the minor reaction pathways are further described.

The heterogeneous loss of HONO by the deposition onto aerosol (ES13-14) surfaces was modeled by

$$k_{HONO\ +\ aerosol} = \frac{\gamma_{HONO}\,\nu_{HONO}}{4}\frac{S_{aerosol}}{V}\frac{RH}{20} \quad \text{(ES13)}$$

$$L_{HONO\ +\ aerosol} = k_{HONO\ +\ aerosol}[HONO] \quad \text{(ES14)}$$

where γ_{HONO} is the calculated irreversible uptake of HONO onto ground surfaces (dimensionless), RH is measured the relative humidity (%), $\frac{S_{ground}}{V}$ is the surface area to volume ratio for the ground surface ($cm^2\ cm^{-3}$), and $\frac{S_{aerosol}}{V}$ is the estimated surface area to volume ratio for the aerosol surface.[5–7]

The vertical and horizontal transport loss processes (L_{trans}) of HONO are represented by a dilution factor (k_{dil}) set to 60-min.[12]

$$L_{trans} = k_{dil}[HONO] \quad \text{(ES15)}$$

Minor loss pathways through the oxidation of HONO by O_3 (ES16) and reaction with itself (ES17) are modeled as

$$L_{HONO+O_3} = k_{HONO+O_3}[HONO][O_3] \quad \text{(ES16)}$$

$$L_{HONO+HONO} = k_{HONO+HONO}[HONO] \quad \text{(ES17)}$$

where L_{HONO+O_3} is the loss of HONO by the oxidation by O_3 (ppb h^{-1}), k_{HONO+O_3} is the rate constant for the reaction between HONO and O_3 (5.0×10^{-19} cm^3 $molecules^{-1}$ s^{-1}),[13] $L_{HONO+HONO}$ is the loss of HONO through the self-reaction (ppb h^{-1}), $k_{HONO+HONO}$ is the rate constant for the reaction between HONO and another HONO molecule (5.8×10^{-25} cm^3 $molecules^{-1}$ s^{-1}),[1] and $[O_3]$ is the measured O_3 mixing ratio (ppb). These minor loss pathways were combined in the main paper as L_{other} (ES18).

$$L_{other} = L_{HONO+aerosol} + L_{HONO+OH} + L_{HONO+O_3} + L_{HONO+HONO} \quad \text{(ES18)}$$

Table S1: Measured compounds and parameters used as model constraints within F0AM and respective measurement methods and data sources.

F0AM Model Designation	Parameter Description	Instrument or Data Source
T	Temperature	Vaisala HMP60
RH	Relative humidity	Vaisala HMP60
JNO2	Photolysis rate constant of NO_2	Metcon 2π Actinic Filter Radiometer
O3	Ozone	Teledyne Model 400E
NO	Nitric oxide	2016 University of Houston
NO2	Nitrogen dioxide	Thermo Model 42C
HONO	Nitrous acid	LP-LIF
OH	Hydroxyl radical	IU-FAGE-LIF
H2	Hydrogen gas	Atmospheric background
C5H8	Isoprene	Agilent 7890B GC-FID; Markes International Unity Series 2 thermal desorber
APINENE	α-pinene	2016 PROPHET G5 Tower
BENZENE	Benzene	2016 PROPHET G5 Tower
TOLUENE	Toluene	2016 PROPHET G5 Tower
MACR	Methacrolein	2016 PROPHET G5 Tower
MVK	Methyl Vinyl Ketone	2016 PROPHET G5 Tower
LIMONENE	Limonene	2016 PROPHET G5 Tower

Table S2: Summary of heterogeneous chemistry parameters used in the F0AM modeling.

Parameter	Description	Equation	Value	Units	Reference
γ_{NO_2}	Uptake coefficient of NO_2	$5.5 \times 10^{-8} \times RH + 7.4 \times 10^{-7}$	$\sim 10^{-6}$	Unitless	[14,15]
$\gamma_{NO_2,hv}$	Photoenhanced uptake coefficient of NO_2	Constant	2×10^{-5}	Unitless	[16]
γ_{HONO}	Uptake coefficient of HONO	$\varphi_{pH} + \varphi_{RH}$	$\sim 5 \times 10^{-4}$	Unitless	This study
φ_{pH}	pH dependence of HONO uptake	$3.604 \times 10^{-6} pH^2 - 4.21 \times 10^{-5} pH + 1.549 \times 10^{-4}$	$\sim 10^{-5}$	Unitless	[17]
φ_{RH}	Relative humidity dependence of HONO uptake	$2.0 \times 10^{-4} \times RH^{-0.043}$	$\sim 10^{-4}$	Unitless	[18–20]
β	Photoenhancement factor	$\frac{J_{NO_2\ max}}{J_{NO_2\ min}}$	$\sim 5 \times 10^{-3}$	Unitless	
EF	Nitric acid photolysis enhancement factor	Constant	30	Unitless	[3]
BLH	Boundary layer height	$BLH_{day} = 3BLH_{night}$	$BLH_{day} = 600$	m	[21,22]

ν_i	Molecular velocity of species i (e.g. HONO, NO_2)	$\sqrt{\frac{3RT}{M_i}}$	~390	m s^{-1}	[23]
$\frac{S_{ground}}{V}$	Surface area to volume ratio for ground	$\frac{2.2}{BLH}$	~10^{-3}	m^{-1}	[6,7]
$\frac{S_{aerosol}}{V}$	Surface area to volume ratio for aerosols	Constant	10^{-4}	cm^2 cm^{-3}	[6,7]

Table S3: Production (P) and loss (L) reaction mechanisms included in the base model and new model.

Reaction Name	Model Name	Equation	Base Model	New Model
Homogeneous Gas Phase Production	P_{OH+NO}	$k_{OH+NO}[OH][NO]$	✓	✓
NO_2 Conversion on Aerosol Surface	$P_{aerosol}$	$\frac{\gamma_{NO_2} \nu_{NO_2}}{4} \frac{S_{aerosol}}{V} [NO_2]$		✓
Photoenhanced NO_2 Conversion on Aerosol Surface	$P_{aerosol+hv}$	$P_{aerosol} \frac{\gamma_{NO_2,hv}}{\gamma_{NO_2}} \frac{J_{NO_2}}{\beta}$		✓
NO_2 Conversion on Ground Surface	P_{ground}	$\frac{\gamma_{NO_2} \nu_{NO_2}}{8} \frac{S_{ground}}{V} \frac{RH}{50} [NO_2]$		✓
Photoenhanced NO_2 Conversion on Ground Surface	$P_{ground+hv}$	$P_{ground} \frac{\gamma_{NO_2,hv}}{\gamma_{NO_2}} \left(\frac{J_{NO_2}}{\beta}\right)^3$		✓
Photolysis of Adsorbed HNO_3	P_{HNO_3+hv}	$J_{HNO_3}[HNO_3]EF$		✓
Hydroperoxyl-Water Complex	$P_{HO_2 \cdot H_2O+NO_2}$	$k_{HO_2 \cdot H_2O+NO_2}[HO_2 \cdot H_2O][NO_2]$		✓
HO_2NO_2 Decomposition	$P_{HO_2NO_2}$	$k_{HO_2NO_2}[HO_2NO_2]$		✓
Photolysis of Orthonitrophenols	$P_{C_6H_5NO_3+hv}$	$J_{C_6H_5NO_3}[C_6H_5NO_3]$		✓
NO_x Hydrolysis	P_{NO_x}	$k_{NO+NO_2+H_2O}[NO][NO_2][H_2O]$		✓
Photolysis	$L_{HONO+hv}$	$J_{HONO}[HONO]$	✓	✓
Transport/Dilution	L_{trans}	$k_{dil}[HONO]$		✓
Ground Deposition	$L_{HONO+ground}$	$\frac{\gamma_{HONO} \nu_{HONO}}{8} \frac{S_{ground}}{V} \frac{RH}{20} [HONO]$		✓
Aerosol Deposition	$L_{HONO+ground}$	$\frac{\gamma_{HONO} \nu_{HONO}}{4} \frac{S_{aerosol}}{V} \frac{RH}{20} [HONO]$		✓

Homogeneous Gas Phase Loss	$L_{HONO+OH}$	$k_{HONO+OH}[HONO][OH]$	✓	✓
Oxidation by Ozone	L_{HONO+O_3}	$k_{HONO+O_3}[HONO][O_3]$		✓
Self-Reaction	$L_{HONO+HONO}$	$k_{HONO+HONO}[HONO]$		✓

Table S4: Summary of descriptive statistics for the main measured species during the MOBCAT field campaign.

Statistic	**HONO** (ppt)	**OH** (10^6 cm^{-3})	**NO_2** (ppb)	**O_3** (ppb)	**JNO_2** (10^{-4} s^{-1})	**RH (%)**	**T (°C)**	**pH**
Mean	19.8	0.83	2.25	20.3	1.35	78.1	19.7	5.98
Minimum	6.7	0.01	0.19	4.1	0.00	33.7	8.8	5.52
Maximum	51.9	2.98	7.18	45.4	14.36	99.7	31.2	6.19
Standard deviation (1σ)	8.6	0.76	1.10	10.0	2.06	17.2	4.5	0.22

Table S5: Summary of the range of HONO measurements at various heights from previous field campaigns at the PROPHET site.

Measurement Dates	**Measurement Height (m)**	**HONO Range (ppt)**	**Reference**
August 5-15, 1998	29.5	90-200	[24]
July 29, 2000	34	~75-300	[25]
July 29, 2000	5	~50-150	[25]
July 30-August 6, 2007	Free troposphere (> 1 km)	4-17	[26]
July 30-August 6, 2007	Boundary layer (< 1 km)	8-70	[26]
July 17-August 7, 2008	~32	~20-200	[27]
July 25-Aug 12, 2022	0.45	6.6-51.9	This study

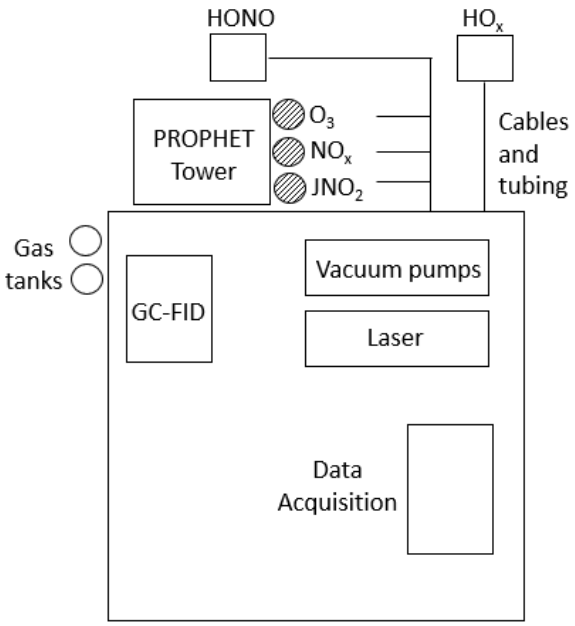

Figure S1: Sampling set up for HONO and OH detection cell at the base of the PROPHET Tower along with supporting measurements.

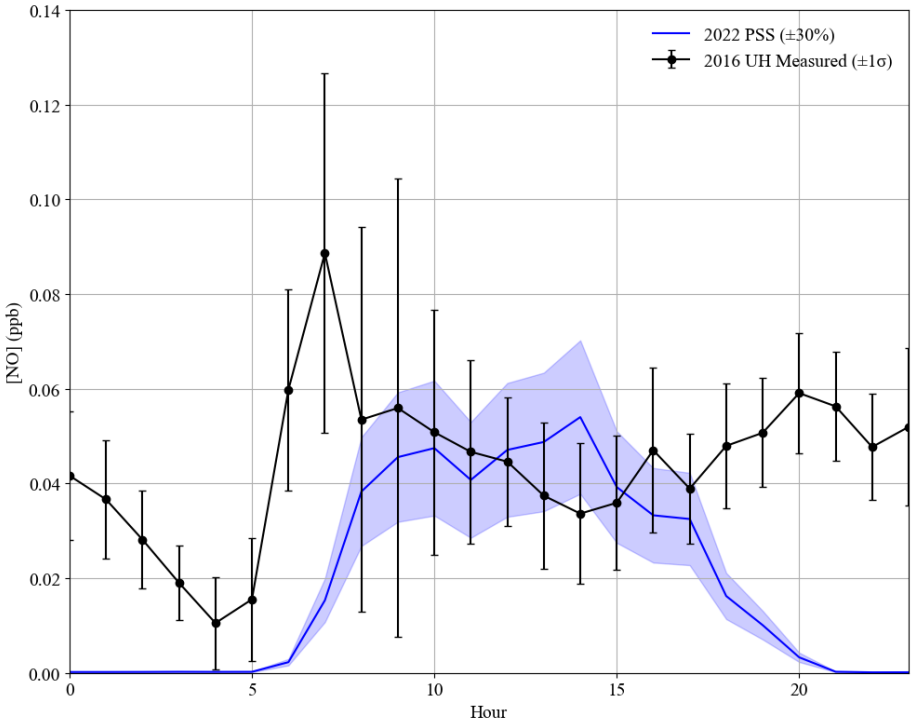

Figure S2: Comparison between the measured 2016 below-canopy NO (black, ±1σ) and the 2022 below-canopy calculated photostationary state (PSS) NO (blue, ±30%).

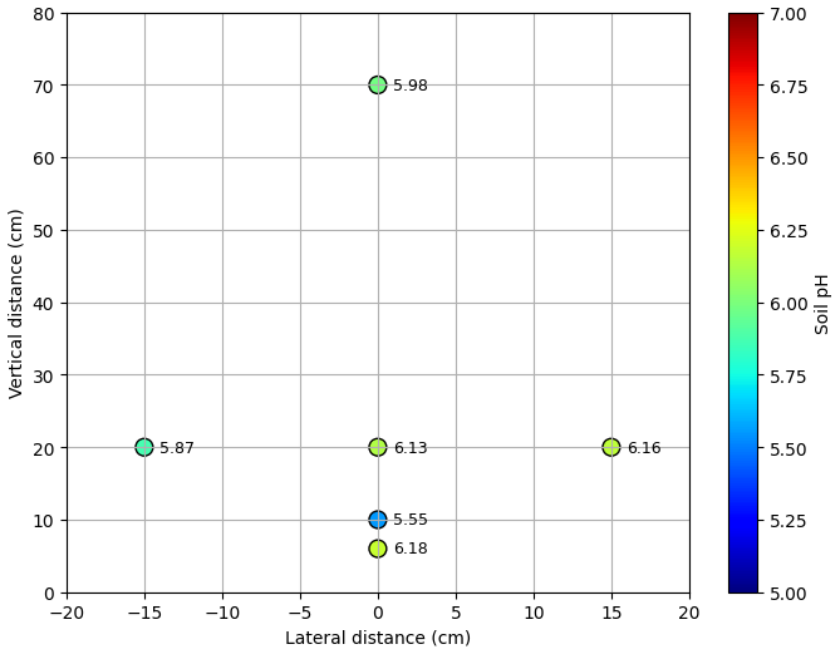

Figure S3: Six soil sampling locations relative to the detection cell and the measured pH (average = 5.98).

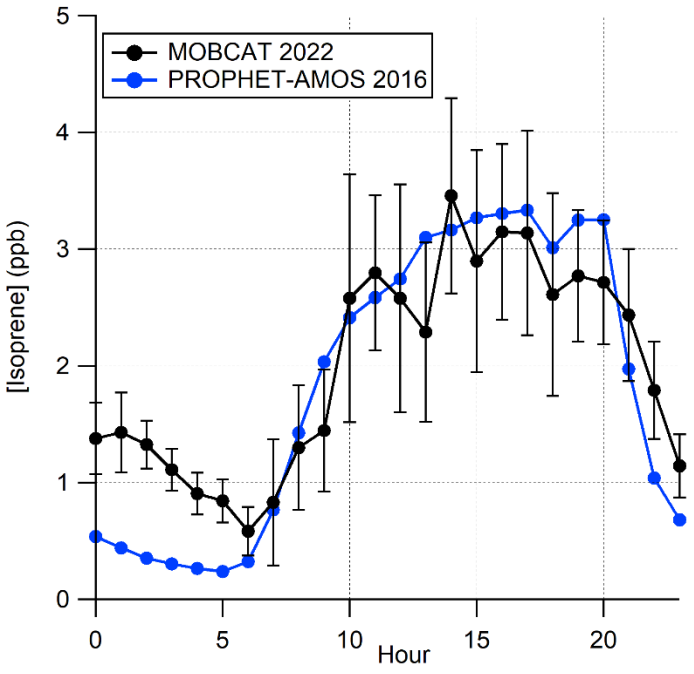

Figure S4: Comparison between measured the isoprene during the MOBCAT 2022 field campaign (black) and during the PROPHET-AMOS 2016 field campaign (blue).[2] Errors bars represent one standard deviation of variability ($\pm 1\sigma$).

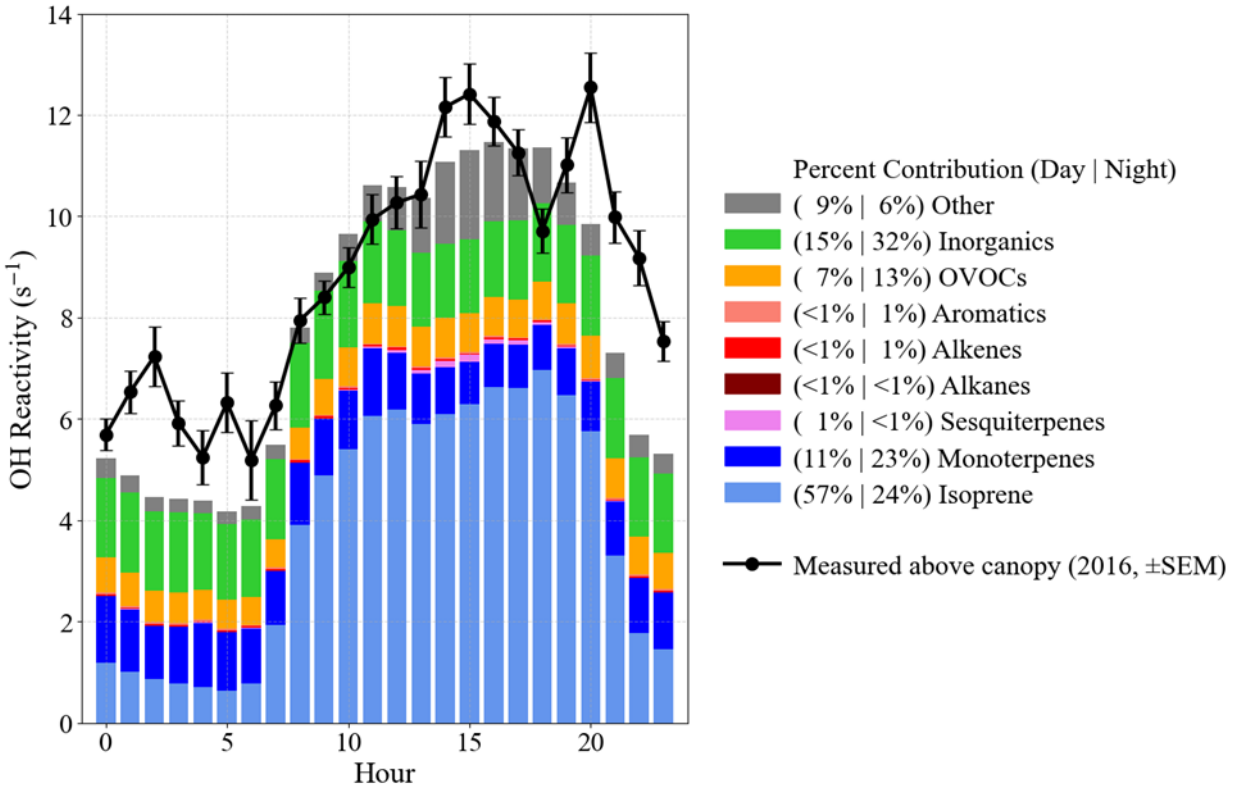

Figure S5: Modeled OH reactivity based on the measured isoprene and previous measurements of monoterpenes and oxygenated VOCs. Relative and overall magnitudes are shown by stacking loss mechanisms for all field campaign data. The black line represents measurements from above the forest canopy (25.6 m) conducted previously at this site in 2016.[2] The lifetime of chemical species (k_{dil}) is set to 60 minutes. Error bars represent the standard error of the mean (SEM).

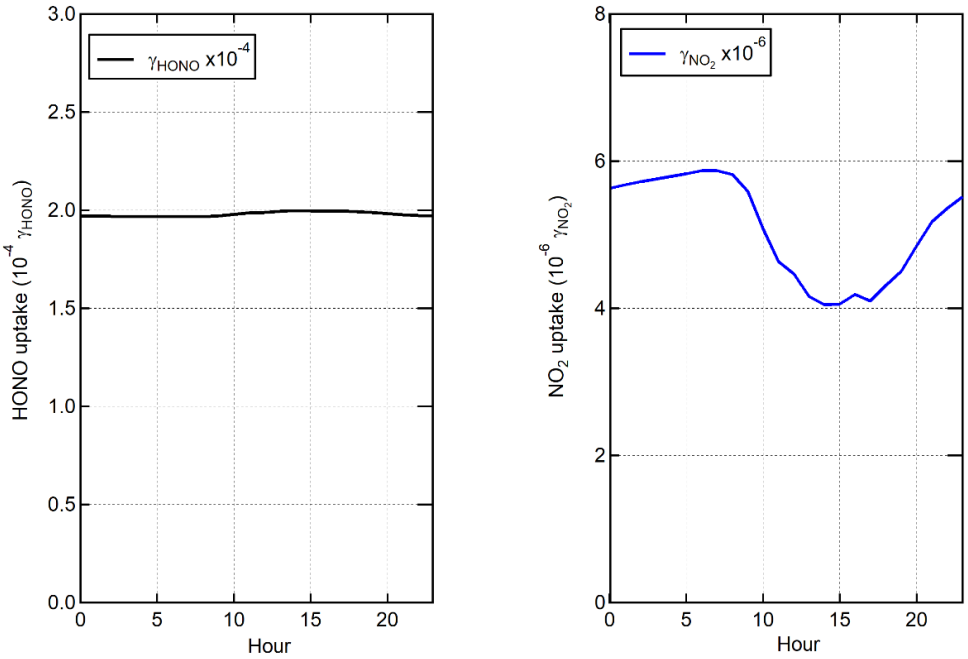

Figure S6: Comparison between the calculated HONO (left, black) and NO_2 (right, blue) uptake coefficients based on the pH and relative humidity dependence. Note the difference in y-axis scales.

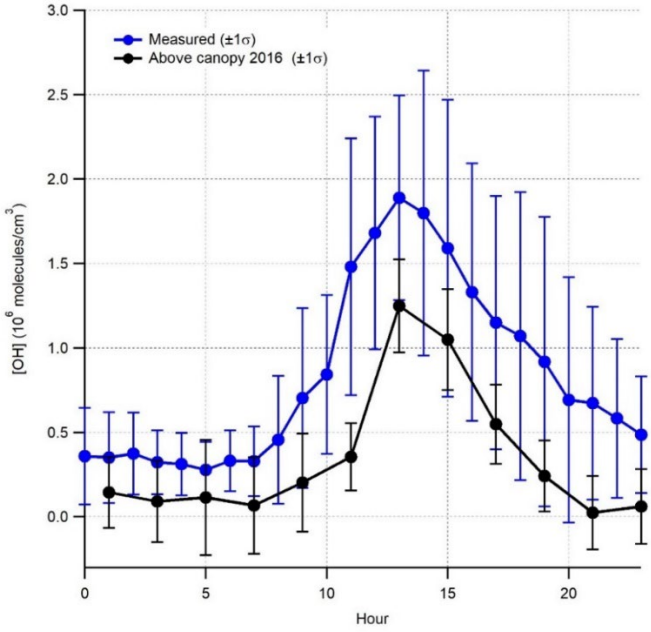

Figure S7: Comparison between below canopy measurements of OH concentrations during the MOBCAT 2022 and the above canopy measurements during PROPHET-AMOS 2016.[2] Error bars represent one standard deviation of variability (±1σ).

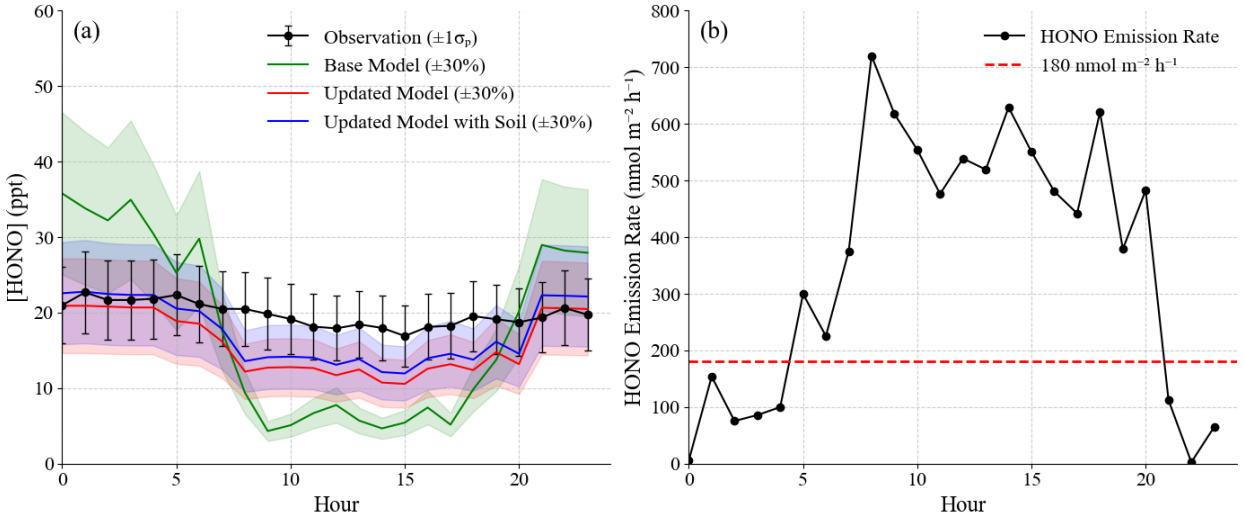

Figure S8: Panel (a) shows the measurements (black), base model (gas phase only, green), updated model with heterogeneous chemistry (red), and the updated model with a constant HONO soil emission rate of 180 nmol m^{-2} h^{-1} (blue). Panel (b) shows the hourly HONO emission rate (black) required to match the difference between the model and observation compared to previous measurements (dashed red).

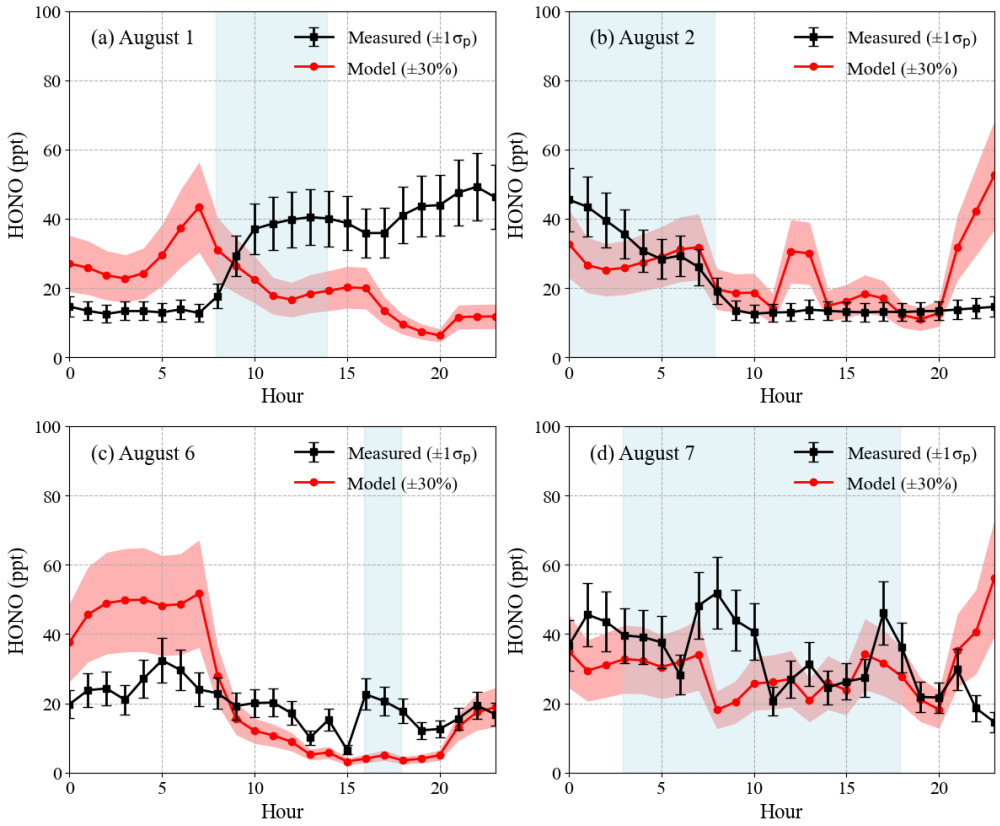

Figure S9: Measured (black) and modeled (red) HONO mixing ratios during rain events (blue shading) on August 1st (a), 2nd (b), 6th (c), and 7th (d).

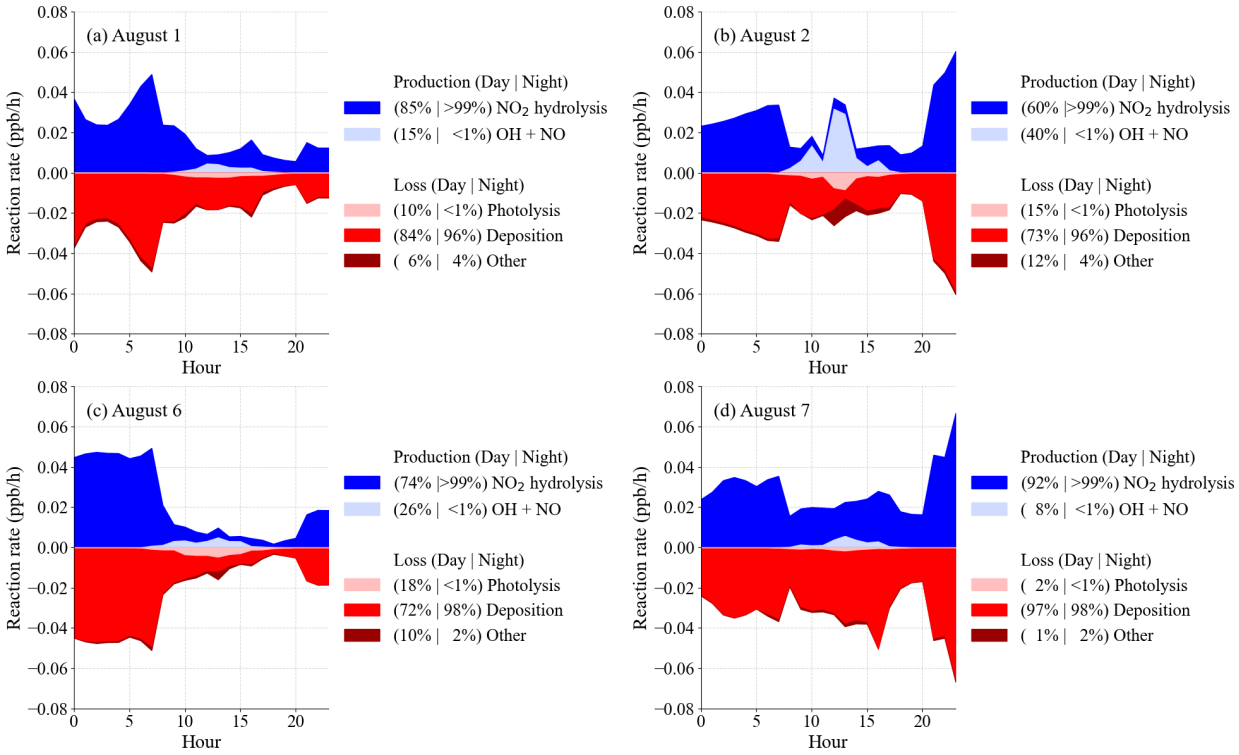

Figure S2: HONO budget for the adjusted model with average daytime (08:00-20:00) and nighttime (20:00-08:00) contributions of each production (blue) and loss (red) reaction rates during precipitation events on August 1st (a), 2nd (b), 6th (c), and 7th (d). Other production and loss mechanisms were negligible.

Supplemental References

1 J. B. Burkholder, S. P. Sander, J. P. D. Abbatt, J. R. Barker and C. Cappa, *Jet Propuls. Lab.*
2 B. Bottorff, M. M. Lew, Y. Woo, P. Rickly, M. D. Rollings, B. Deming, D. C. Anderson, E. Wood, H. D. Alwe, D. B. Millet, A. Weinheimer, G. Tyndall, J. Ortega, S. Dusanter, T. Leonardis, J. Flynn, M. Erickson, S. Alvarez, J. C. Rivera-Rios, J. D. Shutter, F. Keutsch, D. Helmig, W. Wang, H. M. Allen, S. Bertman and P. S. Stevens, *Atmos Chem. Phys.*, 2023, **23**, 10287–10311.
3 P. S. Romer, P. J. Wooldridge, J. D. Crounse, M. J. Kim, P. O. Wennberg, J. E. Dibb, E. Scheuer, D. R. Blake, S. Meinardi, A. L. Brosius, A. B. Thames, D. O. Miller, W. H. Brune, S. R. Hall, T. B. Ryerson and R. C. Cohen, *Environ. Sci. Technol.*, 2018, **52**, 13738–13746.
4 Y. Song, Y. Zhang, C. Xue, P. Liu, X. He, X. Li and Y. Mu, *Environ. Pollut.*, 2022, **311**, 119967.
5 T. C. VandenBoer, S. S. Brown, J. G. Murphy, W. C. Keene, C. J. Young, A. A. P. Pszenny, S. Kim, C. Warneke, J. A. de Gouw, J. R. Maben, N. L. Wagner, T. P. Riedel, J. A. Thornton, D. E. Wolfe, W. P. Dubé, F. Öztürk, C. A. Brock, N. Grossberg, B. Lefer, B. Lerner, A. M. Middlebrook and J. M. Roberts, *J. Geophys. Res. Atmos*, 2013, **118**, 10,155-10,171.
6 D. Li, L. Xue, L. Wen, X. Wang, T. Chen, A. Mellouki, J. Chen and W. Wang, *Atmos. Environ.*, 2018, **182**, 296–306.
7 Y. Liu, Y. Zhang, C. Lian, C. Yan, Z. Feng, F. Zheng, X. Fan, Y. Chen, W. Wang, B. Chu, Y. Wang, J. Cai, W. Du, K. R. Daellenbach, J. Kangasluoma, F. Bianchi, J. Kujansuu, T. Petäjä, X. Wang, B. Hu, Y. Wang, M. Ge, H. He and M. Kulmala, *Atmos Chem. Phys.*, 2020, **20**, 13023–13040.
8 C. Ye, X. Zhou, D. Pu, J. Stutz, J. Festa, M. Spolaor, C. Cantrell, R. L. Mauldin, A. Weinheimer and J. Haggerty, *Science*, 2015, **348**, 1326–1326.
9 J. D. Lee, L. K. Whalley, D. E. Heard, D. Stone, R. E. Dunmore, J. F. Hamilton, D. E. Young, J. D. Allan, S. Laufs and J. Kleffmann, *Atmos Chem. Phys.*, 2016, **16**, 2747–2764.
10 I. Bejan, Y. A. E. Aal, I. Barnes, T. Benter, B. Bohn, P. Wiesen and J. Kleffmann, *Phys. Chem. Chem. Phys.*, 2006, **8**, 2028–2035.
11 W. H. Chan, R. J. Nordstrom, J. G. Calvert and J. H. Shaw, *Environ. Sci. Technol.*, 1976, **10**, 674–682.
12 M. B. Dillon, M. S. Lamanna, G. W. Schade, A. H. Goldstein and R. C. Cohen, *J. Geophys. Res. Atmos*.
13 W. Liao, A. Hecobian, J. Mastromarino and D. Tan, *Atmos. Environ.*, 2006, **40**, 17–26.
14 Y. Liu, K. Lu, X. Li, H. Dong, Z. Tan, H. Wang, Q. Zou, Y. Wu, L. Zeng, M. Hu, K.-E. Min, S. Kecorius, A. Wiedensohler and Y. Zhang, *Env. Sci Technol*, 2019, **53**, 3517–3525.
15 C. Xue, C. Zhang, C. Ye, P. Liu, V. Catoire, G. Krysztofiak, H. Chen, Y. Ren, X. Zhao, J. Wang, F. Zhang, C. Zhang, J. Zhang, J. An, T. Wang, J. Chen, J. Kleffmann, A. Mellouki and Y. Mu, *Environ. Sci. Technol.*, 2020, **54**, 11048–11057.
16 L. Zhang, T. Wang, Q. Zhang, J. Zheng, Z. Xu and M. Lv, *J. Geophys. Res. Atmos*, 2016, **121**, 3645–3662.
17 M. A. Donaldson, D. L. Bish and J. D. Raff, *Proc. Natl. Acad. Sci.*, 2014, **111**, 18472–18477.
18 M. A. Donaldson, A. E. Berke and J. D. Raff, *Environ. Sci. Technol.*, 2014, **48**, 375–383.
19 A. El Zein, M. N. Romanias and Y. Bedjanian, *Environ. Sci. Technol.*, 2013, **47**, 6325–6331.
20 M. N. Romanias, A. El Zein and Y. Bedjanian, *J. Photochem. Photobiol. Chem.*, 2012, **250**, 50–57.

21 K. W. Wong and J. Stutz, *Atmos. Environ.*, 2010, **44**, 3753–3760.
22 B. Hu, J. Duan, Y. Hong, L. Xu, M. Li, Y. Bian, M. Qin, W. Fang, P. Xie and J. Chen, *Atmospheric Chem. Phys.*, 2022, **22**, 371–393.
23 B. J. Finlayson-Pitts and J. N. Pitts, *Chemistry of the Upper and Lower Atmosphere: Theory, Experiments, and Applications*, Academic Press, 2000.
24 T. Thornberry, M. A. Carroll, G. J. Keeler, S. Sillman, S. B. Bertman, M. R. Pippin, K. Ostling, J. W. Grossenbacher, P. B. Shepson, O. R. Cooper, J. L. Moody and W. R. Stockwell, *J. Geophys. Res. Atmos*, 2001, **106**, 24359–24386.
25 X. Zhou, Y. He, G. Huang, T. D. Thornberry, M. A. Carroll and S. B. Bertman, *Geophys. Res. Lett.*
26 N. Zhang, X. Zhou, P. B. Shepson, H. Gao, M. Alaghmand and B. Stirm, *Geophys. Res. Lett.*
27 N. Zhang, X. Zhou, S. Bertman, D. Tang, M. Alaghmand, P. B. Shepson and M. A. Carroll, *Atmospheric Chem. Phys.*, 2012, **12**, 8285–8296.